Fabrication and Characterization of Cellulose Acetate-Based Nanofibers and Nanofilms for H_2S Gas Sensing Application

Nour S. Abdel Rahman [a], Yaser E. Greish [b,c], Saleh T. Mahmoud [d,*], Naser N. Qamhieh [d], Hesham F. El-Maghraby [b,c], Dagou Zeze [e]

[a] Department of Chemical Engineering, UAE University, Al Ain, United Arab Emirates
[b] Department of Chemistry, UAE University, Al Ain, United Arab Emirates
[c] Department of Ceramics, National Research Centre, NRC, Cairo, Egypt
[d] Department of Physics, UAE University, Al Ain, United Arab Emirates
[e] Department of Engineering, Durham University, Durham, United Kingdom

* **Corresponding author.**

Saleh T. Mahmoud, PhD

Professor of Physics,

Department of Physics

UAE University,

Email: saleh.thaker@uaeu.ac.ae,

Tel.: +971-3713-6334, Al Ain P. O. Box 15551,

United Arab Emirates.

Abstract

Electrospun nanofibers and solution-casting nanofilms were produced from an environmentally friendly cellulose acetate (CA) blended with glycerol (as an ionic liquid (IL)), mixed with polypyrrole (PPy, a conducting polymer) and doped with tungsten oxide (WO_3) nanoparticles. The sensing membranes fabricated were used to detect H_2S gas at room temperature and shown to exhibit high performance. The results revealed that the lowest operating temperature of both nanofiber and nanofilm sensors was 20^oC, with a minimum gas detection limit of 1 ppm. Moreover, the sensor exhibits a reasonably fast response, with a minimum average response time of 22.8 and 31.7 s for the proposed nanofiber and nanofilm based sensors, respectively. Furthermore, the results obtained indicated an excellent reproducibility, long-term stability, and low humidity dependence. Such distinctive properties coupled with an easy fabrication technique provide a promising potential to achieve a precise monitoring of harmful H_2S gas in both indoor and outdoor atmospheres.

Keywords: Cellulose acetate, Polypyrrole; H_2S sensor; organic-inorganic hybrid nanocomposites.

1. Introduction

Environmental pollution has become a significant issue worldwide due to the growing industrial waste emission to the community (Lu et al., 2017). Toxic gases such as hydrogen Sulfide (H_2S), carbon monoxide (CO) and ammonia (NH_3) are recognized as environmentally dangerous gaseous pollutants (Kaur et al., 2008; Marszałek, Kowalski & Makara, 2018; Ryu, Arifin, Ha & Lee, 2015). H_2S is of a particular interest since it is one the most hazardous and harmful gases. H_2S is colorless, highly toxic, poisonous, corrosive, flammable and explosive (Beauchamp et al., 1984). It is progressively produced from the anaerobic decomposition of organic materials or other industrial activities including food processing, cooking ovens, kraft paper mills, and petroleum refineries (Ma et al., 2008; Sukunta et al., 2017; Gong et al., 2006). If inhaled, H_2S can cause unconsciousness or death, even at very low concentrations (Mokhatab & Poe, 2012; Yamazoe, 2005).

Consequently, it is essential to monitor H_2S in different settings in real-time and develop highly efficient H_2S sensors in-situ for both industrial and domestic applications (Sun, Yuan, Lium Han & Zhang, 2005). Different methods have been developed to measure trace levels of H_2S in air. The measurement techniques most widely used include gold film analyzers, SO_2 conversion, colorimetric gas detection tubes, electrochemical detectors, and lead acetate cassette tape gas detectors. However, each of them has clear advantages and drawbacks (Deuchar, 2003; Joshi et al., 2014; Pandey, Kim & Tang, 2012; Miura, Yan, Lu & Yamazoe, 1996; Kroll, Smorchkov & Nazarenko, 1994; Khan et al., 2017; Engel, Tarantik, Pannek & Wöllenstein, 2019). Semiconducting metal oxides have been known for decades as good gas sensing materials because of their high sensitivity to many target gases, low cost, and easy fabrication methods. Semiconducting metal oxides (MOSs) such as (Fe_2O_3, CuO, and WO_3) have been widely used for gases and vapors sensing (Tiemann, 2007). In the last few years, nanostructures of metal oxides were found to be effective as gas-sensing materials because of their high surface area that contributes to improving significantly gas detection performance (Afzal, Cioffi, Sabbatini & Torsi, 2012; Sberveglieri et al., 2007; Mirzaei & Neri, 2016; Wetchakun et al., 2011). Among these, WO_3 (tungsten oxide), an n-type metal oxide, exhibits compelling advantages for H_2S gas sensing applications, by virtue of its structure, surface morphology, defect structure, and active surface area, which greatly affect gas sensing properties (Wang et al., 2016; Yin et al., 2019; Kim et al., 2018). However, MOS-based gas sensors including WO3 suffer mainly from high operating

temperatures (∼150−300 °C) that lead to high power consumption and result in a short lifetime [Ali *et.al.,* 2019]. In recent years, different strategies for room-temperature operation using especial morphologies have been introduced in an attempt to address the issue of high-power consumption for resistance-based sensors [Sanjit *et.al.,* 2021]. One of these strategies involves the development of new sensors based on organic conducting polymers with the functionality and conductivity level required to improve gas sensing performance. Such efforts aim at reducing electrical power consumption using low temperatures to maintain their long-term performance and to achieve large-scale production [Kaushik, *et.al.,* 2015]. Intrinsically conducting polymers (ICPs), the so-called "fourth generation of polymeric materials" have been recognized as a new class of organic conducting polymers with remarkable mechanical and electrical properties (Heeger, 2001). ICPs, such as polyacetylene (PA), PPy and polyaniline (PANi) contain monomers that are capable of gaining positive or negative charge through oxidation or reduction. This phenomenon largely contributes to the intrinsic electrical conductivity of the ICPs (Abdelhamid & Snook, 2002; Nambiar & Yeow, 2011). ICPs play an important role in different commercial applications, particularly in actuators, sensors, and electrochromic devices (Smela, 1999; Van de Leur & Van der Waal, 1999; Kincal, Kumar, Child & Reynolds, 1998). For instance, significant research effort has been devoted to PPy due to its good environmental stability, easy synthesis and greater conductivity compared to other ICPs (Ma, Sg, Pr & Shashwati, 2011; Cho et al., 2005).

On the other hand, ionic liquids (ILs) are considered as promising materials for numerous applications (Shokouhi, Adibi, Jalili, Hosseini-Jenab & Mehdizadeh, 2010). Generally, ILs are well known for their good ionic conductivity attained at room temperature and low vapor pressure values (Wei & Ivaska, 2008; Nádherná, Opekar, Reiter & Štulík, 2012; Li, Liu, Pei, Wang & He, 2012). Furthermore, ILs are considered environmentally friendly materials (Li, Liu, Pei, Wang & He, 2012). Such exclusive properties make ILs suitable for the production of electrochemical sensors (Ayesh, Abu-Hani, Mahmoud & Haik, 2016) but also to enhance the ionic conductivity of less conductive polymer (Ayesh, Qadri, Baboo, Hai & Haik, 2013).

Significant research has been directed toward employing nanostructured materials for gas sensing applications. Among various classes of nanostructures, one-dimensional nanomaterials, e.g. ''nanofibers (NFs)'', exhibit an excellent potential for use in gas sensing due to their large surface-to-volume ratio and high interconnected porosity [Ramakrishna et.al., 2006, Mercante et. al., 2019]. This work focuses on producing nanofibers from semiconducting organic polymer

blended with inorganic metal-oxide nanoparticles to detect H_2S gas at low temperature and low detection limit. The sensors fabricated operate at room temperature with detection a limit of 1 ppm and a fast response time of 22.8 - 31.7 s.

In our previous studies, hybrid (inorganic-organic) membranes were successfully developed and evaluated as H_2S gas sensors. In these studies, combinations of semiconducting nanoparticles (WO_3 and CuO) were used in a matrix of a conductive polymer (Chitosan, PVA) and with the help of an ionic liquid, synergistically provided a mechanism of detecting H_2S gas at low temperatures. The proposed sensor assembly is an organic-inorganic nanocomposite, i.e. a hybrid structure that has attracted much attention for the development of sensing applications (Wang & Shannon, 2011). The uniqueness and novelty of the proposed hybrid structure is in the combined contribution of its carefully selected components and the conducting nature of the environmentally friendly and sustainable CA and to the role played by the ionic liquid acting as a facilitator of charge transfer within the matrix (Ju, Park, Jung & Lee, 2009; Allam, Ayesh, Mohsin & Haik, 2013). Moreover, the presence of intrinsically conducting PPy particulates and semiconducting WO_3 nanoparticles ensures a smooth charge transfer and provide an added value for the overall sensor construct (Geng et al., 2006; Su & Peng, 2014; Ali, Awwad, Greish, Abu-Hani & Mahmoud, 2020; Abu-Hani, Greish, Mahmoud, Awwad & Ayesh, 2017). Furthermore, the sensor fabricated in our previous work [Hittini et. al., 2020] is highly affected by the relative humidity and the response of the sensor was around 12% at 20% relative humidity. The current sensors exhibited a low humidity dependence, and the responses of the nanofiber and nanofilm-based sensors are 15% -20% at 80% humidity, respectively. Thus, this sensor has the potential to work in a harsh environment. The proposed sensor assembly is shown to exhibit enhanced features compared with similar sensors reported in the literature.

2. Experiment

2.1. Materials

Tungsten Oxide (WO_3, 99% hydrolyzed), cellulose acetate (CA, MW 50,000 and 35% acetyl content), polypyrrole (PPy, conductivity 10-50 S/cm), acetone, dimethylacetamide (DMAc), and glycerol (IL) were purchased from Sigma Aldrich-USA.

2.2. Preparation of (PPy-IL- WO_3 NPs-CS) solution

Composite sensor mixtures were prepared in three separate 100-ml beakers based on the WO_3 NPs proportions. In each beaker, 0.24 g of glycerol (IL) was added to 40 ml of DMAc/Acetone (1:2)

solvent mixture and thoroughly mixed. 5, 7.5, and 10 wt.% of WO_3 NPs (in proportion to CA used) were subsequently added to the individual solutions to vary the concentration of WO_3 NPs. This was followed by the addition of PPy, 2wt.% with respect to CA used before magnetic stirring was applied until homogeneous suspensions were obtained. 4.8 g of CA was gradually and slowly added (time of addition is 5 hours) to each suspension and subjected to a continuous vigorous stirring for 24 h until clear homogeneous solutions were achieved. The amount of IL used was calculated to be 5wt.% of CA while the CA concentration was 12wt.% of the solution's total volume. The solutions prepared were used for the fabrication of nanofilm and nanofibers-based sensor membranes denoted hereafter as PPy-IL-WO_3 NPs-CA.

2.3. Preparation of (2 wt% PPy-IL-10 wt% WO_3-CA) nanofilm-based sensor

To prepare the sensing nanofilms with different WO_3 concentration, a fixed volume of each of the homogenous solutions was cast on a Teflon plate to form a thin membrane, then dried in a vacuum oven at 50^{o}C for 12 h. A non-porous cast film with a high degree of flexibility was obtained, as shown in Fig. 1. Uniform composite membranes of around 1.7 mm thickness were obtained.

2.4. Preparation of (2 wt% PPy-IL-10 wt% WO_3-CA) nanofiber-based sensor

To prepare the fibers, a constant volume of 10 ml of each of the homogenous solutions was fed into a plastic syringe, then electrospun into nanofibers at ambient conditions using NANOSPINNER24 equipment. A set of pre-optimized electrospinning parameters was used, including a stainless steel needle with 21 gauge, a spinning distance (needle tip to collector distance) of 15 cm, an applied voltage of 20 kV between the tip and the grounded collector, and a constant flow rate of 0.5 ml/h. The electrospun fibrous membranes obtained were in the form of flexible sheets, which were dried further at 50^{o}C for 12 h.

2.5. Characterization

The morphologies of the as-received PPy powder and the nanofibrous films prepared thereafter were investigated using scanning electron microscopy (SEM: JEOL, JSM-5600). In addition, an energy-dispersive X-ray spectrometer (EDS) was used to confirm the presence and the homogeneity of the WO_3-PPy-CA composite fibrous membranes. The size of the WO_3 particle was obtained using a Zetasizer (Malver Instruments, Model ZEN360, United Kingdom).

2.6. Sensor fabrication

Each sensor was fabricated and connected electrically as explained elsewhere (Abu-Hani, Awwad, Greish, Ayesh & Mahmoud, 2017). A square piece (1×1 cm^2) of the composite film/fiber was cut

and placed between a 0.15 μm thick copper bottom contact (1.5×1.5 cm^2) and a stainless steel grid (0.8×0.8 cm^2) with a mesh size of 250×250 μm^2 as the top contact. Stainless steel was chosen for the top contact because it is anti-corrosive, therefore, resistant H_2S. A conductive silver paste was used to fix the three layers, acting as an efficient heatproof adhesive.

2.7. H_2S Gas sensing test

The sensor fabricated was placed on a hot plate inside a temperature-controlled Teflon chamber. The bottom and top parts of the device were connected by 2 electrical feed-troughs. Furthermore, a Bronkhorst mass flowmeter was used to control the flow rate of the gases. Before the injection of the H_2S gas into the chamber, the gas was diluted with a fixed proportion of air with flow rate of 200 sccm using a gas mixer such that the concentration of the H_2S gas becomes 1, 10, 15, 25 and 50 ppm. The sensors developed were subsequently exposed to H_2S inside the temperature-controlled Teflon chamber. The tests were conducted under atmospheric pressure inside a fume hood and at different temperatures 20, 40, and 60^oC (measured at the copper sheet's surface). All tests (current-voltage: I–V) were performed by applying a fixed bias voltage of 2.0 V across the sensor electrodes and the electrical current was measured as a function of time using a Keithley Instruments source measurement unit (KI 236). All I-V measurements were performed in triplicates (n=3) to ensure a statistical relevance of the data recorded. The gas flow meters, controller, and KI 236 were interfaced to a computer using LABVIEW software. The relative humidity inside the test chamber was 0% (dry gas) unless stated otherwise. A detailed schematic diagram of the gas testing system is provided in our previous work (Hittini et al., 2020).

3. Results and Discussion

3.1.Morphology and structural characteristics

The as-received PPy conducting polymer was analyzed for its structure and composition using SEM-EDS**.** The PPy particulates showed a uniform granularity with a high purity and an elemental composition of C and N, as confirmed by the EDS analysis. The average size of the PPy particulates is approximately 0.9 μm, with a unimodal particle size distribution obtained by particle size analysis. The WO_3 NPs used in this work were characterized for their composition and morphology in our previous study (Ali, Awwad, Greish, Abu-Hani & Mahmoud, 2020). The average size of the WO_3 NPs was 140-200 nm, as measured by Diameter J software (Ali, Awwad, Greish, Abu-Hani & Mahmoud, 2020).

To produce a non-beaded nanofibrous sensor membrane, the optimum proportion of PPy initially added to the CA solution prior electrospinning was evaluated. Accordingly, three PPy concentrations; 2, 5, and 7wt.%, were studied. An optimum proportion of 2wt% of the PPy particulates was selected since non-beaded nanofibers with a homogeneous fiber size distribution were achieved thereafter. However, increasing the proportion of the PPy particulates resulted in the presence of beads in the nanofibrous films. This is attributed to the increased viscosity of the PPy-CA suspension with the addition of PPy particulates, which in turn affects the electrospinnability of the suspension (Jeun et al., 2007). This optimum PPy particulates concentration was used for the preparation of the nanofibrous and nanofilm membranes at constant IL and CA concentrations for 5, 7.5, and 10wt.% WO_3 NPs intake.

Fig. 1(a-c) show the SEM micrographs of the CA nanofibrous electrospun membranes containing 2wt.% PPy and 5 vol.% IL for three different concentrations of WO_3 NPs (5, 7.5, and 10wt.% WO_3). Increasing WO_3 concentration from 5 to 10wt.%, causes an increase in the initial viscosity of the solutions, which was reflected in an increase in the fiber's diameter, as illustrated by Fig. 1. It is a well-known fact that the diameter of the nanofibers fabricated by electrospinning are greatly influenced by the polymer concentration and the viscosity of the solution. Under the same electrospinning conditions, increasing the polymer concentration causes an increase in solution viscosity. Hence, increasing the viscosity of the solution increases the diameter of the nanofibers [J. Lasprilla-Botero, M. Álvarez-Láinez, and J.m.Lagaron, 2018, Y. Yang, R. He, Y. Cheng, and N. Wang, 2020]. Composite membranes containing 5 and 7.5wt% WO_3 are characterized by an average fiber size of 350 nm and 500 nm, respectively. However, a membrane with 7.5wt% WO_3 exhibited a heterogeneous fiber size distribution. In turn, 10wt% WO_3 in the nanofibrous membrane led to 400 nm average fiber size with a homogeneous fiber size distribution. On the other hand, the increase in the dimensions of the nanofibers led to a decrease in the porosity of the membranes. These results are in a good agreement with the data presented in our previous work [Hittini et., al., 2020]. Moreover, increasing the concentration of WO_3 NPs to 10wt% led to an increase in the reactive sites within the fibrous sensing membrane and hence improves the response of the sensor. Therefore, the sensors made with 10wt% WO_3 shows a noticeable improvement in the sensor's response due to high porosity and more reactive sites in the sensing membrane compared with 5 and 7.5wt% of WO3 NPs. The presence of the WO_3 NPs and PPy particles was further confirmed by elemental analysis (EDS) of the fibrous membrane containing the highest concentration of WO_3 NPs (10wt.%), as shown in Fig. 1(d). Accordingly, an optimum

concentration of 10wt.% of WO_3 NPs in the CA fibrous membranes was selected to study the sensing characteristics of the membranes prepared.

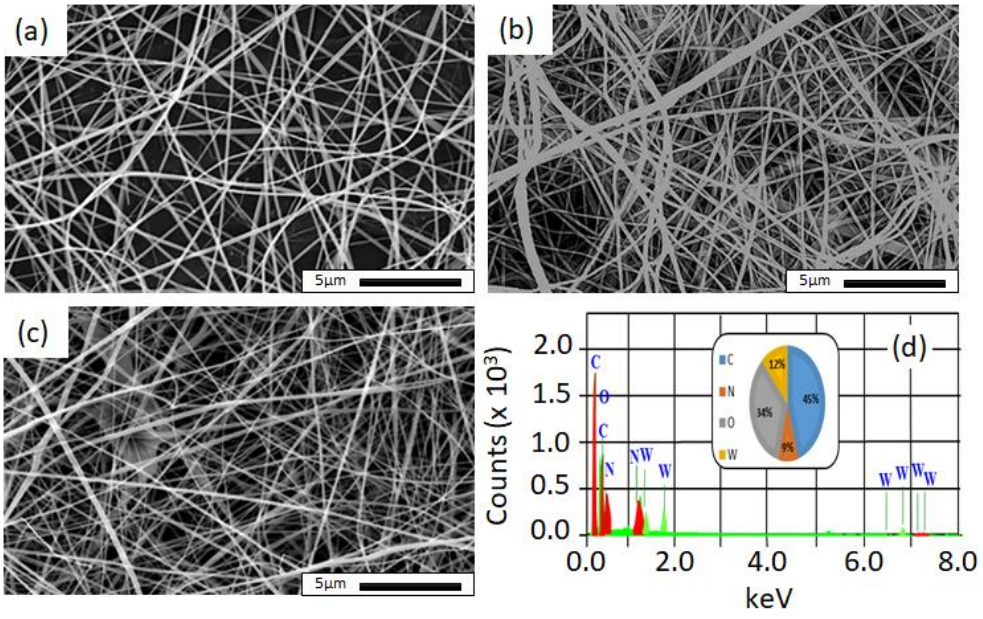

Fig. 1. SEM images of (a) PPy-IL-5wt% WO_3-CA nanofibers. (b) PPy-IL-7.5wt% WO_3-CA nanofibers, (c) PPy-IL-10wt% WO_3-CA nanofibers, and (e) EDS spectra of PPy-IL-10wt% WO_3-CA nanofibers.

Fig. 2(a-c) show the microstructure of the nanofilms prepared, with an approximate average thickness of 1.7 mm. In addition, all nanofilms showed the same degree of flexibility, while a homogeneous distribution of the PPy and WO_3 particles was confirmed.

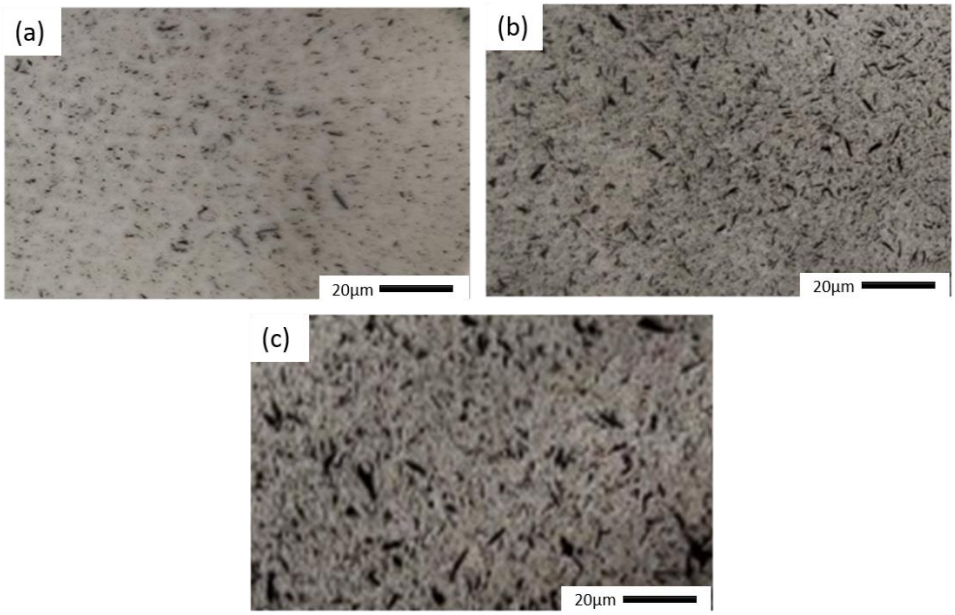

Fig. 2. SEM micrographs of the prepared sensing nanofilms containing; (a)10wt% WO_3 , (b) 7.5wt% WO_3, and (c) 5wt% WO_3.

3.2. Electrical characteristics

Since the operating temperature plays a major role in the gas sensing performance, the I-V characteristics of the composites prepared were evaluated at three different operating temperatures: 20, 40, and 60^{o}C. Fig. 3 (a & b) displays typical I-V curves as a function of temperature for the PPy-IL-10wt.% WO_3-CA nanofilm and nanofiber samples, respectively. These I-V curves are almost linear but have a slight nonlinearity and vary with the operating temperature as expected. Such I-V performance is attributed to the increase in the electrical charge carriers conduction path induced by the addition of IL and the NPs. This is in line with the small potential barrier observed between the contact and the polymer membrane (Liu, Adhikari, Guo & Adhikari, 2013). In addition, the PPy conductive polymer particulates present in the polymer matrix also contributes to increasing the conductivity observed. Such phenomena facilitate charge carriers transport once the sensor is exposed to H_2S gas (Nguyen & El-Safty, 2011; Ayesh, Mahmoud, Qamhieh & Karam, 2014).

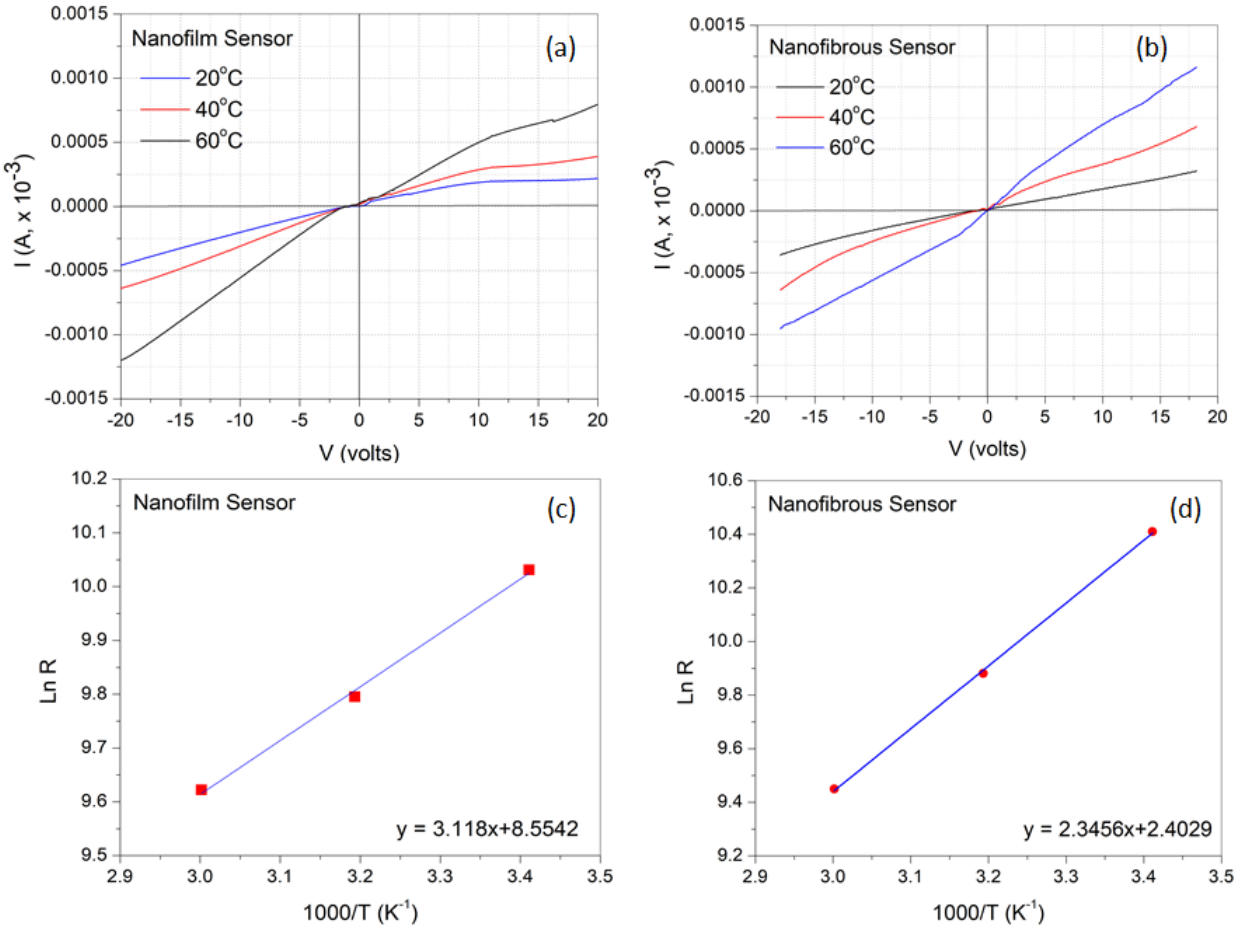

Fig. 3. Electrical characteristics of (2 wt% PPy-IL-10 wt% WO_3-CA) sensors; (a) I-V curve for nanofilm sensor. (b) I-V curve for nanofiber sensor. Dependence of the resistance (Ln(R)) on the temperature (1000/T) for nanofilm based sensor (c) and nanofiber-based sensor (d).

Fig. 3 (c & d) show the dependence of the sensor's resistivity (Ln(R)) on the reciprocal of temperature (1000/T) (K^{-1}) for the nanofilm and nanofiber-based sensors. The resistance decreases linearly as the temperature increases, which is attributed to the increase in the number of the free charge carriers in the conduction band due to thermal excitation (Mironenko et al., 2016). Consequently, a linear fit of the curves was used to determine the activation energy (E_a) of each sensor following Arrhenius equation (Eq. 1) (Jensen, 1985):

$$R = R_o e^{\frac{E_a}{k_B T}} \quad (1)$$

Where, Ro is a pre-exponential factor, k_B the Boltzmann constant, and T the temperature. The activation energy extracted for the nanofilm and nanofiber-based sensors were 0.270 and 0.202 eV, respectively. The relatively lower activation energy for the nanofiber sensor compared with

that of the nanofilm sensor could be attributed to the higher surface area of the nanofibers sensing element as compared with that of the nanofilm sensing element, even though both sensing elements contain the same constituents. As a first approximation, the activation energy can be seen as the difference between the conduction band and the Fermi energy level, $E_a = E_C - E_F$. Since the surface area of the nanofiber-based sensor is bigger than that of the nanofilm-based sensor, a higher surface defect states are expected. The creation of these defects alters the density of states in the forbidden energy gap, which shifts the Fermi level towards the conduction band edge and lowers the activation energy as a result. It should be mentioned that low activation energies are highly desirable since it enhances the sensor's response to H_2S gas presence and recovery time while decreasing the operating temperature (Korotcenkov, 2007). The low activation energies observed could be attributed to the inter-particle electron movement from WO_3 to PPy at the heterojunctions, where a positively charged depletion layer is formed on the WO_3 surface. This phenomenon, not only contributes to the reduction of the activation energy, but it also results in a reduction in the enthalpy of the physical adsorption of gases, thus showing excellent electron-donating characteristics (Geng et al., 2006; de Lacy Costello, Evans, Ewen, Honeybourne & Ratcliffe, 1996).

Depending on the data shown in Fig. 3 (a & b), a constant biased voltage (2.0 V) was calculated from the linear part of the I-V curves, and was applied across the sensors' electrodes in order to avoid any current saturation (Ali, Mahmoud, Awwad, Greish & Abu-Hani, 2020). Accordingly, the I-V response was measured as a function of the gas concentration, time and temperature as shown later in the current study.

3.3. Gas sensing properties

The performance of the nanofiber and nanofilm sensors obtained with the chemical composition of PPy-IL-10wt.% WO_3-CA was investigated for the detection of H_2S gas. The sensor was prepared and inserted inside the gas test chamber as discussed in section 2.7. A fixed bias of 2.0 V was applied to establish a background current in the sensor before the sensor was exposed to for different concentrations of H_2S gas (1-50 ppm). The corresponding current response signal was measured as a function of time. Fig. 4 represents the sensor's time dependent-current response at 40^{o}C for the PPy-IL-10wt.% WO_3-CA nanofiber sample. These results indicate that the current measured increases significantly, as the sensor is exposed to increasing concentrations of H_2S. These changes in the current correspond to a decrease in the resistance, which is attributed to the

proton doping effect associated with PPy particulates and is further supported by the characteristics of WO_3 NPs as an established n-type semiconductor (Geng, 2010).

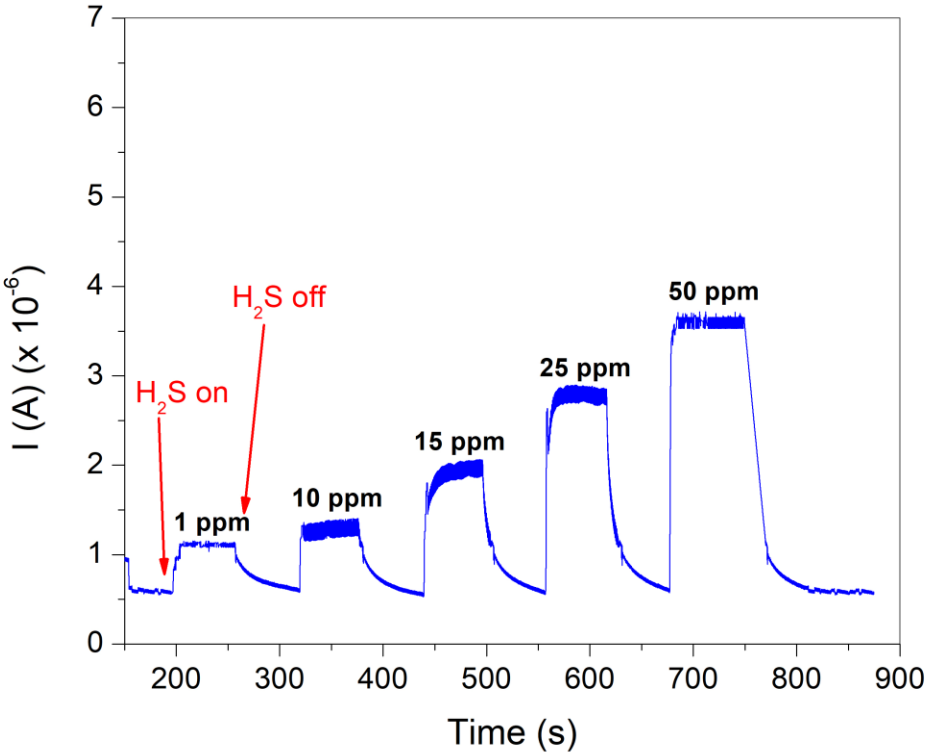

Fig. 4. A representative current response of the (PPy-IL-10 wt% WO_3-CA) nanofiber-based sensor as function of the time and H_2S concentrations.

Furthermore, a reversible behavior of the sensor performance is clearly revealed, where the current recovers its initial value once the H_2S gas flow is closed and the residual H_2S pumped out. This behavior demonstrates the reproducibility of the sensors fabricated and the ability to use them several times without adversely altering their accuracy. Fig. 4 also indicates very clearly that the magnitude to the sensor's response is proportional to the gas concentration, where the higher the H_2S gas concentration, the higher the current value measured. The sensor's response to H_2S is defined by Eq. 2 and calculated at each operating temperature:

$$S(\%) = \frac{|I_g - I_a|}{I_a} \times 100 \quad (2)$$

Where, I_a is the reference current of the sensor measured in air, and I_g the current of the sensor exposed to the test gas (mainly H_2S).

During the test, H_2S was diluted with air inside the gas mixer and injected into the test chamber at various H_2S concentrations: 1-50 ppm. Furthermore, the flow rate was controlled, while the

operating temperature was varied at 20, 40, and 60°C. Fig. 5 (a & b) displays the sensor's response (S%) as a function of operating temperature and H_2S concentrations for both nanofibers and nanofilms-based sensors, respectively. All measurements were performed in triplicates at a fixed temperature and gas concentration.

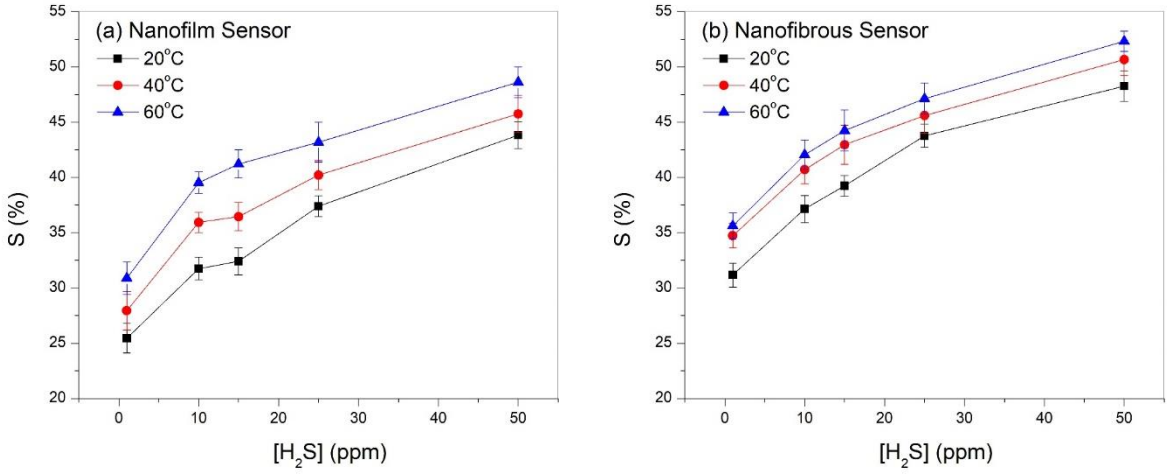

Fig. 5. Sensor's response for H_2S gas of: (a) (PPy-IL-10 wt% WO_3-CA) nanofilm base sensor, and (b) (PPy-IL-10 wt% WO_3-CA) nanofiber based sensor, at different H_2S concentrations and operating temperatures.

The results show a high response to H_2S gas, even at a low temperature of 20°C. Likewise, the response of the sensors is directly proportional to the gas concentrations and temperatures inside the test chamber. For instance, as Fig. 5 (b) demonstrates that when the H_2S concentration was increased from 10 to 25 ppm at a constant operating temperature, the response increases by 17.7%. Whereas, at a constant H_2S concentration the sensor's response showed an increase of 13.2% when the temperature was increased from 20 to 40°C. This could be attributed to the presence of both WO_3 NPs and PPy particulates, which largely contribute to the conductivity of the sensor that is further improved by increasing the operating temperature (Abu-Hani, Greish, Mahmoud, Awwad & Ayesh, 2017). These results also indicate a high reliability of the sensor fabricated as the error bars of the sensor's response are within a low standard deviation. A minimum detection limit of 1 ppm was achieved at all operating temperatures. It is very essential to notice a reasonable response at low temperature (20°C) for all sensors fabricated, making the proposed sensor membranes suitable to detect very low H_2S concentrations. As such these sensors can protect workers running the risk of a direct and dangerous exposure to H_2S on daily basis.

3.4. Sensor performance

To confirm the reliability of the sensors produced, four parameters were evaluated, i.e. selectivity, response time, stability (reproducibility) and humidity. Each sensor was tested individually in triplicates (n=3). The response time is a very significant criterion to evaluate the performance of the sensors obtained. The response time is defined as the time needed to reach 90% of the sensor's maximum response. Fig. 6 (a & b) presents the response time for the nanofilm and nanofiber-based sensors as a function of the temperature and WO_3 NPs intake in both types of sensors. These results indicate that the nanofilm-based sensor show a minimum average response time of 24.49 s at 60°C, and a maximum average response time of 31.65 s at 20°C. On the other hand, the nanofiber sensor showed a shorter minimum average response time of 16.56 s at 60°C, and a maximum average response time of 22.81 s at 20°C. The faster response time for the nanofiber-based sensor is attributed to the higher surface area of the sensing material, unlike the non-fibrous nanofilm sensor. However, it should be noted that the response of the sensors developed are faster than those mentioned in the literature for similar sensors used for the detection of H_2S gas (Geng et al., 2006; Su & Peng, 2014).

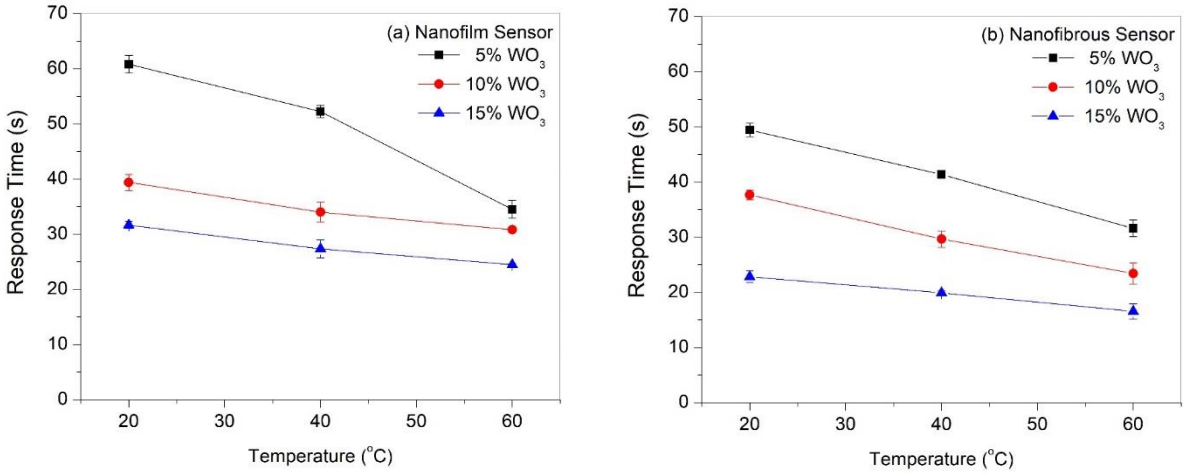

Fig. 6. Response times of the sensors as a function of temperature and WO_3 content for (a) CA-PPy-IL-WO_3 nanofilm based sensor and (b) CA-PPy-IL-WO_3 fiber-based sensor.

To test the reproducibility of the fabricated sensors, each sensor was exposed to a constant H_2S gas concentration of 10 ppm at a constant operating temperature of 40°C for four repeating cycles. The results shown in Fig. 7 (a & b), suggest the responses of the sensors are broadly repeatable

over the four cycles considered for both types of sensors. This is indicative of their good reproducibility in the detection of H_2S. This test was repeated continuously for 10 days and the response (S%) was calculated and presented in Fig. 7(c). For a given temperature and H_2S gas concentration, the repeated response of each sensor was very close to the initial response recorded, which indicates that both sensors fabricated exhibit an excellent long-term stability.

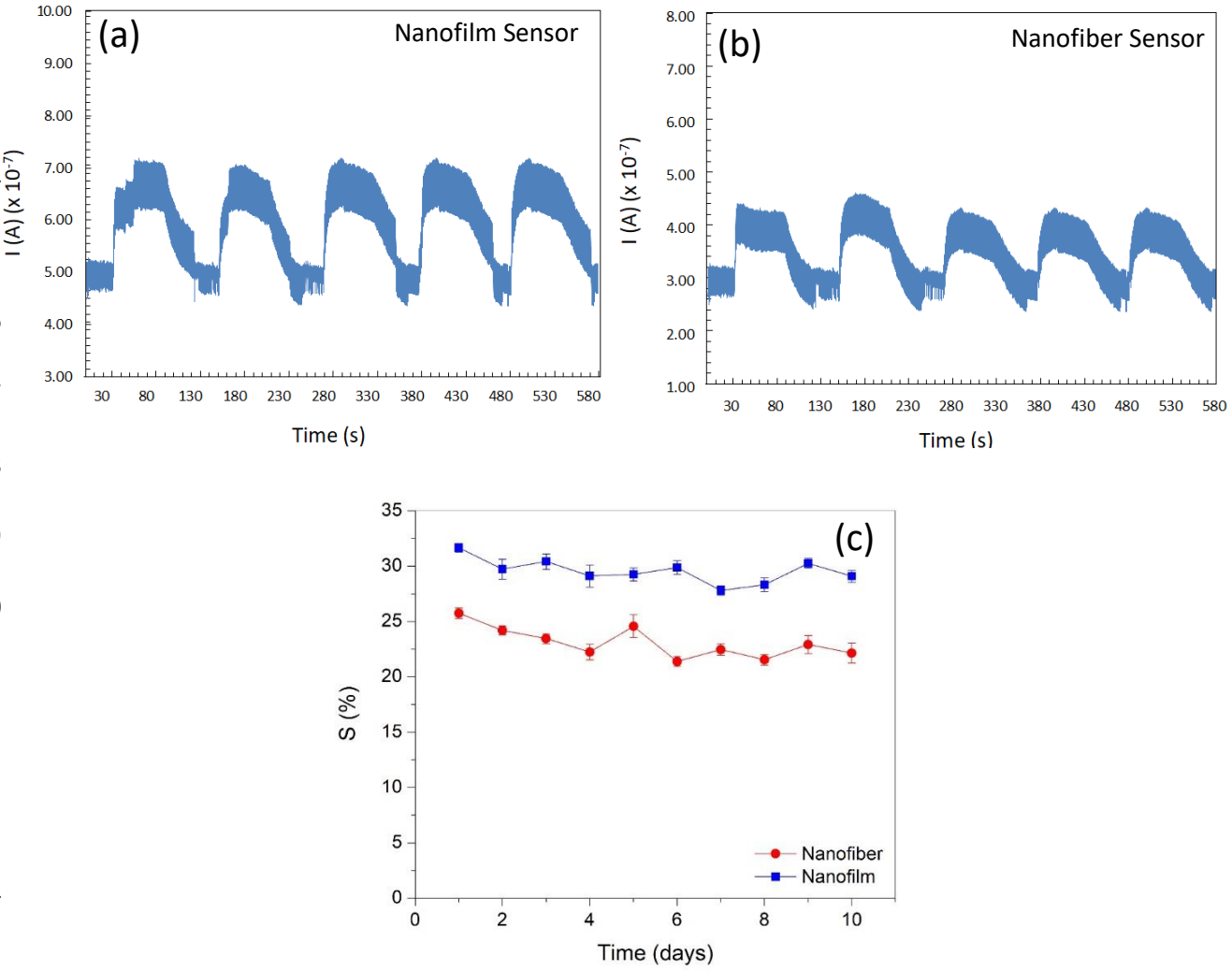

Fig.7. (a) Reproducibility of (PPy-IL-10 wt% WO_3-CA) nanofilm sensor (a) and (PPy-IL-10 wt% WO_3-CA) fiber sensor. (c) Long-term stability of both sensors measured at 40°C.

The selectivity of both sensors was tested, and the results shown in Fig. 8a. The sensors were exposed to three potential interfering gases separately, i.e. hydrogen (H_2), ethylene (C_2H_4), and nitrogen dioxide (NO_2) with a concentration of 200 ppm. The sensor's response to each of these gases was recorded at 40°C. The response (S%) of both sensors to all these gases are very weak (less than 10%), while their response to H_2S was exceptionally high (7-10 times higher), indicating

the high selectivity of the sensors proposed to H_2S gas. The relative humidity limits the reliability of the sensor to detect H_2S gas, since the ambient humidity varies dynamically with changes in the weather, season, and temperature. As such, reducing the dependence of the sensor on the humidity to a low level is highly desirable. The effect of varying the relative humidity inside the test chamber on the sensor's response (S%) was evaluated at 60°C in the presence of 50 ppm H_2S gas, see Fig. 8b. The results reveal that increasing the relative humidity inside the test chamber resulted in a decrease in the response of the sensors. An increase in the relative humidity up to 80% resulted in a 31.6% drop in the response of the sensors. This is expected because of the possible adsorption of water molecules onto the sensing membrane surface through the formation of H-bonding. Hence, the adsorption of H_2S molecules onto the surface of the sensors is limited by the H-bonds (Kruefu, Wisitsoraat, Tuantranont & Phanichphant, 2015).

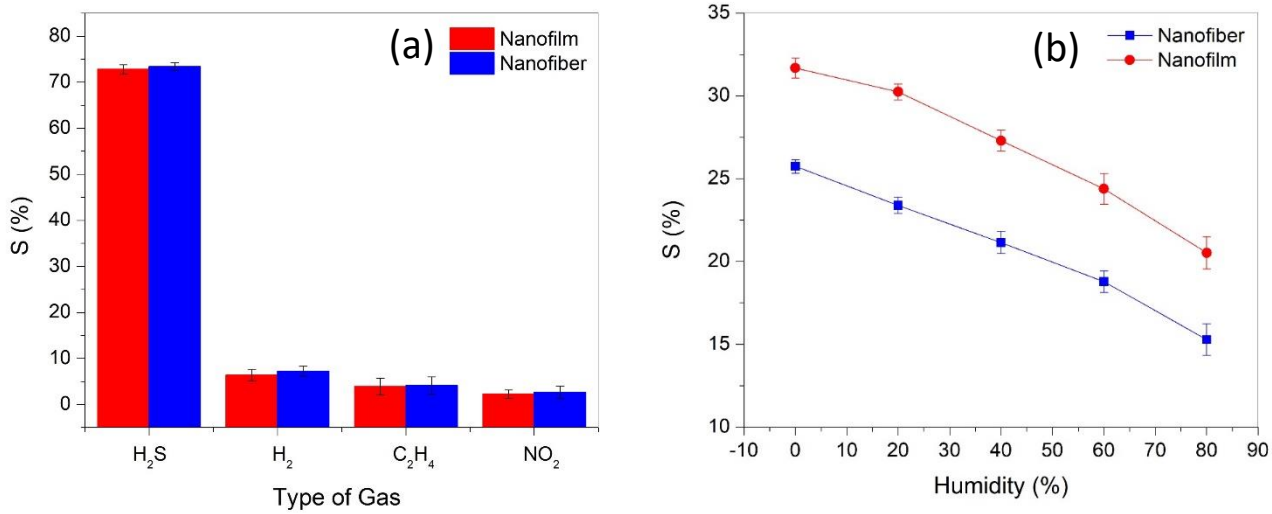

Fig. 8. (a) Selectivity histogram for the PPy+5%IL+10 wt% WO_3-CA sensors for different gases and (b) dependence of the PPy-IL-10 wt% WO_3-CA sensors results on the humidity.

Table 1 contrasts the performance of the sensors developed in the current study is contrasted against those reported in the literature (Geng et al., 2006; Su & Peng, 2014; Geng, 2010). The nanofiber and nanofilm-based sensors presented in this work exhibit a relatively excellent sensing performance compared with those studied previously. This is attributed to their unique composition and method of fabrication. The sensors presented in this work are able to operate at room temperature and yield a very low detection limit of 1 ppm and a fast response time of 22.8 s and 31.7 s for the nanofiber and nanofilm-based devices, respectively. This means that our sensors clearly outperform those requiring higher operating temperatures (90°C) and characterized by a longer response time (70-360 s).

Table 1. *Performance comparison of the developed H_2S gas sensor with the literature for optimum response.*

Composition/ material	Structure	Gas sensing Response (%)	Response Time	Detection limit [H_2S]	Operating temperature	Reference
CA-PPy-IL-10 wt% WO_3	Nanofibers	31.2	22.8 (s)	1 ppm	20 (^oC)	This work
CA-PPy-IL-10 wt% WO_3	Nano film	25.5	31.7 (s)	1 ppm	20 (^oC)	This work
PPy- WO_3	Film	81	360 (s)	1 ppm	RT (^oC)	[44]
PPy-3 wt% WO_3	NCs	61	70 (s)	100 ppm	90 (^oC)	[45]
PPy-1 wt% WO_3	Film	49.55	NA	1000 ppm	90 (^oC)	[60]

3.5. Gas sensing mechanism

The sensing mechanism of semiconductor gas sensors is identified as a surface-controlled in which the particle size, surface states, and oxygen adsorption play an important role in the overall sensing mechanism (Rothschild & Komem, 2004; Rout, Hegde & Rao, 2008). The interaction between the target gas and the surface of the sensing material is the main reason behind the change of the sensor response (Hittini et al., 2020). Therefore, understanding the sensing mechanism for the proposed IL-PPy-WO_3 NPs-CA based sensor is necessary. Generally, when the sensor is exposed to H_2S, it interacts with the gas through the oxygen molecules adsorbed on the surface of the sensing material. As a result, the electrical conductivity (resistance) of the sensing material changes and the variation is detected as a readable current variation as a function of time (Ali, Awwad, Greish, Abu-Hani & Mahmoud, 2020). Initially, the oxygen molecules easily adsorb on the surface of the sensing material; because of their high electron affinity (0.43 eV) (Mane, Suryawanshi, Kim & Moholkar, 2016). The oxygen molecules adsorbed attract electrons from the IL-PPy-WO_3NPs-CA surface. Therefore, oxygen ions adsorbed (O_2^-, $O^{2-}$and O^-) appear on the sensor's surface. The following reactions occur on the sensing material surface (Rout, Hegde & Rao, 2008; Mane, Suryawanshi, Kim & Moholkar, 2016):

$$O_2(g) \rightarrow O_2(ads) \quad (3)$$

$$O_2(ads) + e^- \rightarrow O_2^-(ads) \quad (4)$$

$$O_2^-(ads) + e^- \rightarrow 2O^-(ads) \quad (5)$$

$$O^- + e^- \rightarrow O^{2-}(ads) \quad (6)$$

When the sensors (nanofibers and nanofilms) produced are exposed to H_2S, the oxygen molecules adsorbed interact with H_2S gas, which extract electrons from the conduction band of the WO_3 NPs and trap them at the surface in the form of ions as described in the following reaction (Su & Peng, 2014; Hosseini, Iraji zad & Mortezaali, 2015):

$$2H_2S(g) + 3O_2^-(ads) \rightarrow 2H_2O + 2SO_2 + 3e^- \quad (7)$$

The free electrons released are transferred within the matrix of the composite sensor via the H-bonding network between the remaining components of the sensor; namely the CA matrix (fiber or film), the PPy conducting particulates and the ionic liquid. This results in an overall increase in the conductivity of the sensor, as illustrated schematically in Fig. 9. A similar pattern was previously observed in a composite sensor that was composed of a chitosan matrix in addition to WO_3 NPs and IL (Ali, Awwad, Greish, Abu-Hani & Mahmoud, 2020).

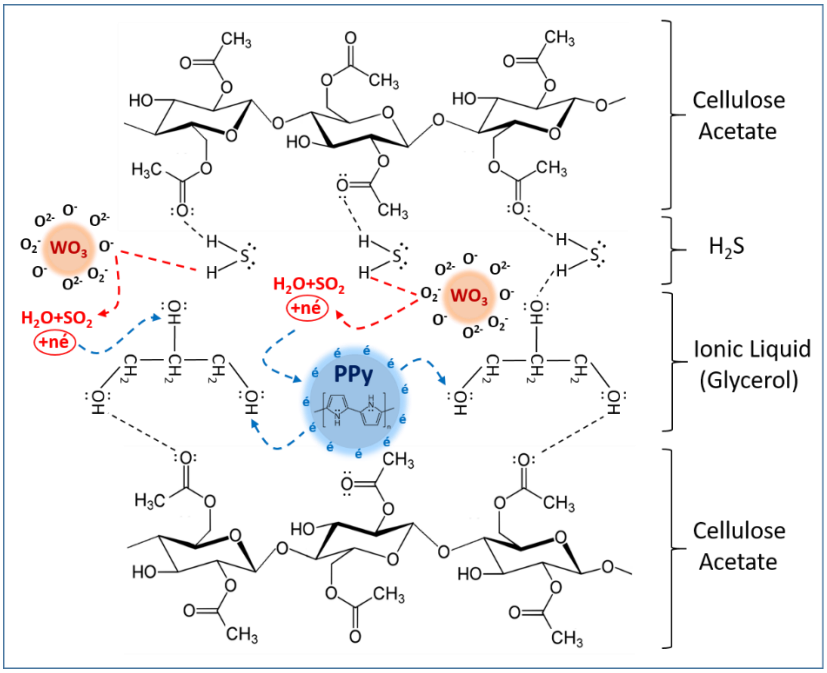

Fig.9. Illustration of the combined contribution of the sensor's components leading to the enhanced sensing of H_2S gas through H-bonding and e-transfer.

On the other hand, when the H_2S gas flow is turned off, the number of free electrons decreases and leads to a reduction in the conductivity of the sensing element, causing a reversible sensing behavior (Abu-Hani, Greish, Mahmoud, Awwad & Ayesh, 2017). The synergistic effect resulting from the co-existence of PPy particulates, WO_3 nanoparticles and a well-established ionic liquid in a matrix that compliments the integration of these components, is considered as the key reason behind the exceptional properties of the proposed sensors (Su & Peng, 2014; Geng, 2010).

4. Conclusion

High-response and room-temperature sensors for H_2S gas detection were successfully fabricated using electrospun nanofibers and solution-casting nanofilms. The proposed sensor assembly consists of cellulose acetate blended with glycerol as an ionic liquid, mixed with a conducting polymer and doped with tungsten oxide nanoparticles. The results of this study confirm that the proposed sensors possess excellent sensing properties, a fast response time and a low detection limit (1 ppm) even at room temperature. The results also demonstrate that the sensors exhibit high selectivity for H_2S gas, long-term stability, and low power consumption. It was also shown that nanofibers-based sensors are more sensitive and selective to detecting H_2S compared with the nanofilm based sensor.

The lowest operating temperature for both nanofibers and nanofilm based sensors was 20^{o}C, with a minimum gas detection limit of 1 ppm. Moreover, both sensors exhibited a reasonably fast response. For instance, for 2wt.% PPy+5%IL+10wt.% WO_3-CA, the average response time is 22.8 ± 1.05 s for nanofibers-based sensors and 31.7±1.3 s for the nanofilm-based sensors. A comparative study with the literature shows that the sensors produced in this work outperform other sensors, which often operate at a higher temperature (90^{o}C) and require a longer response time (70-360 s). The reliability of the sensors was also studied in terms of reproducibility and long-term stability. For a given temperature (e.g. T= 40^{o}C) and H2S (1 ppm) gas, the repeated response of each sensor was very close to the initial value recorded. This indicates the excellent reproducibility and long-term stability of the proposed nanofibers and nanofilms-based sensors. The dependence of the sensor's response S(%) on the relative humidity inside the test chamber at 60^{o}C and 50 ppm was also evaluated. The results revealed a low humidity dependence of the sensors since a reasonable drop in the response occurs only when the relative humidity increases to 80%. Such distinctive properties of the sensors that are based environmentally friendly materials can pave new paths for the development of reliable H_2S sensor to monitor indoor/outdoor pollution.

5. Acknowledgment

The authors would like to acknowledge the financial support by United Arab Emirates University with Grants Codes: USRP-G00003232 with fund code 31R238/activity code R238M4, and UPAR-G00002589-fund code 31S310.

6. References

Abdelhamid, M. & Snook, G. (2002). Conducting Polymers and Their Application in Supercapacitor Devices. *Encyclopedia of Polymer Science and Technology,* pp. 1-20.

Abu-Hani, A., Greish, Y., Mahmoud, S., Awwad, F. & Ayesh, A. (2017). Low-temperature and fast response H_2S gas sensor using semiconducting chitosan film. *Sensors and Actuators B: Chemical,* 253, 677-684.

Abu-Hani, A., Awwad, F., Greish, Y., Ayesh, A. & Mahmoud, S. (2017). Design, fabrication, and characterization of low-power gas sensors based on organic-inorganic nano-composite. *Organic Electronics,* 42, 284-292.

Afzal, A., Cioffi, N., Sabbatini, L. & Torsi, L. (2012). NOx sensors based on semiconducting metal oxide nanostructures: progress and perspectives. *Sensors and Actuators B: Chemical,* 171, 25-42.

Ali, F., Awwad, F., Greish, Y., & Mahmoud, S. (2019). Hydrogen Sulfide (H_2S) gas sensor – A brief review . IEEE Sensors Journal, Vol. 19, Issue 7, PP 2394-2407

Ali, F., Awwad, F., Greish, Y., Abu-Hani, A. & Mahmoud, S. (2020). Fabrication of low temperature and fast response H_2S gas sensor based on organic-metal oxide hybrid nanocomposite membrane. *Organic Electronics,* 76, 105486.

Ali, F., Mahmoud, S., Awwad, F., Greish, Y. & Abu-Hani, A. (2020). Low power consumption and fast response H_2S gas sensor based on a chitosan-CuO hybrid nanocomposite thin film. *Carbohydrate Polymers,* 116064.

Allam, M., Ayesh, A., Mohsin, M. & Haik, Y. (2013). Physical properties of PVA doped with algal glycerol. *Journal of Applied Polymer Science,* 130, 4482-4489.

Ayesh, A., Abu-Hani, A., Mahmoud, S. & Haik, Y. (2016). Selective H_2S sensor based on CuO nanoparticles embedded in organic membranes. *Sensors and Actuators B: Chemical,* 231, 593-600.

Ayesh, A., Qadri, S., Baboo, V., Haik, M. & Haik, Y. (2013). Nano-floating gate organic memory devices utilizing Ag–Cu nanoparticles embedded in PVA-PAA-glycerol polymer, *Synthetic metals,* 183, 24-28.

Ayesh, A., Mahmoud, S., Qamhieh, N. & Karam, Z. (2014). Investigation of charge transport in percolating network of PdCu nanoclusters. *Acta Metallurgica Sinica (English Letters)*, 27, 156-160.

Beauchamp, R., Bus, J., Popp, J., Boreiko, C., Andjelkovich, D & Leber, P. (1984). A critical review of the literature on hydrogen sulfide toxicity. *CRC Critical Reviews in Toxicology*, 13, 25-97

Cho, J., Yu, J., Kim, J., Sohn, S., Lee, D. & Huh, J. (2005). Sensing behaviors of polypyrrole sensor under humidity condition. *Sensors and Actuators B: Chemical*, 108, 389-392.

de Lacy Costello, B., Evans, P., Ewen, R., Honeybourne, C. & Ratcliffe, N. (1996). Novel composite organic–inorganic semiconductor sensors for the quantitative detection of target organic vapours. *Journal of Materials Chemistry*, 6, 289-294.

Deuchar, C. (2003). *The detection and measurement of hydrogen sulphide*. PhD thesis, University of Nottingham.

Engel, L., Tarantik, K., Pannek, C. & Wöllenstein, J. (2019). Screen-Printed Sensors for Colorimetric Detection of Hydrogen Sulfide in Ambient Air. *Sensors*, 19, 1182, 2019.

Geng, L., Huang, X., Zhao, Y., Li, P., Wang, S., Zhang, S. & Wu, S. (2006). H_2S sensitivity study of polypyrrole/WO_3 materials. *Solid-state electronics*, 50, 723-726.

Geng, L. (2010). Gas sensitivity study of polypyrrole/WO_3 hybrid materials to H_2S. *Synthetic metals*, 160, 1708-1711.

Gong, J., Chen, Q., Lian, M., Liu, N., Stevenson, R. & Adami, F. (2006). Micromachined nanocrystalline silver doped SnO_2 H_2S sensor. *Sensors and Actuators B: Chemical*, 114, 32-39.

Heeger, A. (2001). Semiconducting and metallic polymers: the fourth generation of polymeric materials. *J. Phys. Chem. B*, 105, 8475-8491.

Hittini, W., Greish, Y., Qamhieh, N., Alnaqbi, M., Zeze, D. & Mahmoud, S. (2020). Ultrasensitive and low temperature gas sensor based on electrospun organic-inorganic nanofibers. *Organic Electronics, 81,* 105659.

Hosseini, Z., Iraji zad, A. & Mortezaali, A. (2015). Room temperature H_2S gas sensor based on rather aligned ZnO nanorods with flower-like structures. *Sensors and Actuators B: Chemical*, 207, 865-871.

Jensen, F. (1985). Activation energies and the Arrhenius equation. *Quality and Reliability Engineering International*, 1, 13-17.

Jeun, J., Kim, Y., Lim, Y., Choi, J., Jung, C., Kang, P. & Nho, Y. (2007). Electrospinning of Poly (L-lactide-co-D, L-lactide). *Journal of Industrial and Engineering Chemistry*, 13, 592-596.

Joshi, N., Saxena, V., Singh, A., Koiry, S., Debnath, A., Chehimi, M., Aswal, D. & Gupta, S. (2014). Flexible H_2S sensor based on gold modified polycarbazole films. *Sensors and Actuators B: Chemical,* 200, 227-234.

Ju, Y., Park, S., Jung, H. & Lee, W. (2009). Electrospun activated carbon nanofibers electrodes based on polymer blends. *Journal of The Electrochemical Society*, 156, A489-A494.

Kaushik A., Kumar R., Arya, S. K., Nair M., Malhotra B. D., and Bhansali S., (2015). Organic−Inorganic Hybrid Nanocomposite-Based Gas Sensors for Environmental Monitoring Chemical Review, 115, 11, pp 4571–4606.

Kaur, M., Jain, N., Sharma, K., Bhattacharya, S., Roy, M., Tyagi, A., Gupta, S. & Yakhmi, J. (2008). Room-temperature H_2S gas sensing at ppb level by single crystal In_2O_3 whiskers," *Sensors and Actuators B: Chemical,* 133, 456-461

Khan, M., Qazi, F., Hussain, Z., Idrees, M., Soomro, S. & Soomro, S. (2017). Recent trends in electrochemical detection of NH_3, H_2S and NOx gases. *International Journal of Electrochemical Science,* 12, 1711-1733.

Kim, M., Jang, J., Koo, W., Choi, S., Kim, S., Kim, D. & Kim, I. (2018). Bimodally porous WO_3 microbelts functionalized with Pt catalysts for selective H_2S sensors. *ACS applied materials & interfaces,* 10, 20643-20651.

Kincal, D., Kumar, A., Child, D., Reynolds, J. (1998). Conductivity switching in polypyrrole-coated textile fabrics as gas sensors. *Synthetic Metals,* 92, 53-56.

Korotcenkov, G. (2007). Metal oxides for solid-state gas sensors: What determines our choice?. *Materials Science and Engineering: B,* 139, 1-23.

Kroll, A., Smorchkov, V. & Nazarenko, A. (1994). Electrochemical sensors for hydrogen and hydrogen sulfide determination. *Sensors and Actuators B: Chemical,* 21, 97-100.

Kruefu, V., Wisitsoraat, A., Tuantranont, A. & Phanichphant, S. (2015). Ultra-sensitive H_2S sensors based on hydrothermal/impregnation-made Ru-functionalized WO_3 nanorods. *Sensors and Actuators B: Chemical,* 215, 630-636.

Lasprilla-Botero J., Álvarez-Láinez M., and Lagaron J. M. (2018). "The influence of electrospinning parameters and solvent selection on the morphology and diameter of polyimide nanofibers," *Materials Today Communications,* vol. 14, pp. 1-9.

Li, Z., Liu, X., Pei, Y., Wang, J. & He, M. (2012). Design of environmentally friendly ionic liquid aqueous two-phase systems for the efficient and high activity extraction of proteins. *Green Chemistry,* 14, 2941-2950.

Liu, H., Adhikari, R., Guo, Q. & Adhikari, B. (2013). Preparation and characterization of glycerol plasticized (high-amylose) starch–chitosan films. *Journal of Food Engineering,* 116, 588-597.

Lu, Z., Chen, H., Hao, Y., Wang, J., Song, X. & Mok, T. (2017). "The dynamic relationship between environmental pollution, economic development and public health: Evidence from China," *Journal of Cleaner Production,* 166, 134-147

Ma, G., Yan, H., Shi, J., Zong, X., Lei, Z. & Li, C. (2008). Direct splitting of H_2S into H_2 and S on CdS-based photocatalyst under visible light irradiation. *Journal of Catalysis,* 260, 134-140.

Ma, C., Sg, P., Pr, G. & Shashwati, S. (2011). Synthesis and characterization of polypyrrole (PPy) thin films. *Soft nanoscience letters,* 1, 6-10.

Mane, A., Suryawanshi, M., Kim, J. & Moholkar, A. (2016). Highly selective and sensitive response of 30.5% of sprayed molybdenum trioxide (MoO_3) nanobelts for nitrogen dioxide (NO_2) gas detection. *Journal of colloid and interface science,* 483, 220-231.

Marszałek, M., Kowalski, Z. & Makara, M. (2018). Emission of greenhouse gases and odorants from pig slurry-effect on the environment and methods of its reduction, *Ecological Chemistry and Engineering S,* 25, 383-394, 2018

Mercante L. A., Andre R. S., Mattoso L. C., and Correa. D. S. (2019). Electrospun Ceramic Nanofibers and Hybrid-Nanofiber Composites for Gas Sensing. ACS Appl. Nano Mater. 2, 7, 4026–4042.

Mirzaei A. & Neri, G. (2016). Microwave-assisted synthesis of metal oxide nanostructures for gas sensing application: A review. *Sensors and Actuators B: Chemical,* 237, 749-775.

Mironenko, A., Sergeev, A., Nazirov, A., Modin, E., Voznesenskiy, S. & Bratskaya, S. (2016). H_2S optical waveguide gas sensors based on chitosan/Au and chitosan/Ag nanocomposites. *Sensors and Actuators B: Chemical,* 225, 348-353.

Miura, N., Yan, Y., Lu, G. & Yamazoe, N. (1996). Sensing characteristics and mechanisms of hydrogen sulfide sensor using stabilized zirconia and oxide sensing electrode. *Sensors and Actuators B: Chemical,* 34, 367-372.

Mokhatab, S. & Poe, W. (2012) *Handbook of natural gas transmission and processing*. Gulf professional publishing.

Nádherná, M., Opekar, F., Reiter, J. & Štulík, K. (2012). A planar, solid-state amperometric sensor for nitrogen dioxide, employing an ionic liquid electrolyte contained in a polymeric matrix. *Sensors and Actuators B: Chemical,* 161, 811-817.

Nambiar, S. & Yeow, J. (2011). Conductive polymer-based sensors for biomedical applications. *Biosensors and Bioelectronics,* 26, 1825-1832.

Nguyen, H. & El-Safty, S. (2011). Meso-and macroporous Co_3O_4 nanorods for effective VOC gas sensors. *The Journal of Physical Chemistry C,* 115, 8466-8474.

Pandey, S., Kim, K. & Tang, K. (2012). A review of sensor-based methods for monitoring hydrogen sulfide. *TrAC Trends in Analytical Chemistry,* 32, 87-99.

Ramakrishna S., Fujihara K., Teo W. E, Yong T., Ma Z., and Ramasseshan R., (2006). Electrospun nanofibers: solving global issues. Materials Today, Vol. 9, No.3, pp 40-50.

Rothschild, A. Komem, Y. (2004). The effect of grain size on the sensitivity of nanocrystalline metal-oxide gas sensors. *Journal of Applied Physics,* 95, 6374-6380.

Rout, C., Hegde, M. & Rao, C. (2008). H_2S sensors based on tungsten oxide nanostructures, *Sensors and Actuators B: Chemical,* 128, 488-493.

Ryu, S., Arifin, E., Ha, S. & Lee, J. (2015). On-site Colorimetric Forensic Sensor (I): Quantitative Detection of Toxic H_2S and NH_3 Gases Using Metal-Ion-modified Silica Powders. *Bulletin of the Korean Chemical Society,* 36, 2434-2439, 2015.

Sanjit M. M., Ali M., Kim H. W., Kim S. S., Kim T. W., (2021). Recent advances in energy-saving chemiresistive gas sensors: A review. Nano Energy 79, 105369

Sberveglieri, G., Baratto, C., Comini, E., Faglia, G., Ferroni, M., Ponzoni A. & Vomiero A. (2007). Synthesis and characterization of semiconducting nanowires for gas sensing. *Sensors and Actuators B: Chemical,* 121, 208-213.

Shokouhi, M., Adibi, M., Jalili, A., Hosseini-Jenab, M. & Mehdizadeh, A. (2010). Solubility and diffusion of H_2S and CO_2 in the ionic liquid 1-(2-hydroxyethyl)-3-methylimidazolium tetrafluoroborate. *Journal of Chemical & Engineering Data,* 55, 1663-1668.

Smela, E. (1999). Microfabrication of PPy microactuators and other conjugated polymer devices. *Journal of micromechanics and microengineering,* 9, 1-18

Sukunta, J., Wisitsoraat, A., Tuantranont, A., Phanichphant, S. & Liewhiran, C. (2017). Highly-sensitive H_2S sensors based on flame-made V-substituted SnO_2 sensing films. *Sensors and Actuators B: Chemical,* 242, 1095-1107.

Su, P. & Peng, Y. (2014). Fabrication of a room-temperature H_2S gas sensor based on PPy/WO_3 nanocomposite films by in-situ photopolymerization. *Sensors and Actuators B: Chemical,* 193, 637-643.

Sun, Z., Yuan, H., Liu, Z., Han, B. & Zhang, X. (2005). A highly efficient chemical sensor material for H_2S: α-Fe_2O_3 nanotubes fabricated using carbon nanotube templates. *Advanced Materials,* 17, 2993-2997.

Tiemann, M. Porous metal oxides as gas sensors. (2007). *Chemistry - A European Journal,* 13, 8376-8388, 2007.

Van de Leur, R. & Van der Waal, A. (1999). Gas and vapour detection using polypyrrole. *Synthetic Metals,* 102, 1330-1331.

Wang, T. & Shannon, C. (2011). Electrochemical sensors based on molecularly imprinted polymers grafted onto gold electrodes using click chemistry. *Analytica chimica acta,* 708, 37-43.

Wang, Y., Liu, B., Xiao, S. Wang, X., Sun, L., Li, H., Xie, W., Li, Q., Zhang, Q. & Wang, T. (2016). Low-temperature H_2S detection with hierarchical Cr-doped WO_3 microspheres. *ACS applied materials & interfaces*, 8, 9674-9683.

Wei, D., Ivaska, A. (2008). Applications of ionic liquids in electrochemical sensors. *Analytica chimica acta*, 607, 126-135.

Wetchakun, K., Samerjai, T., Tamaekong, N., Liewhiran, C., Siriwong, C., Kruefu, V., Wisitsoraat, A., Tuantranont, A. & Phanichphant, S. (2011). Semiconducting metal oxides as sensors for environmentally hazardous gases. *Sensors and Actuators B: Chemical*, 160, 580-591.

Wu, J., Yang, Y., Yu, H., Dong, X. & Wang, T. (2019). Ultra-efficient room-temperature H_2S gas sensor based on $NiCo_2O_4$/r-GO nanocomposites. *New J. Chem*., 43, 10501.

Yamazoe, N. (2005). Toward innovations of gas sensor technology. *Sensors and Actuators B: Chemical*, 108, 2-14.

Yang Y., He R., Cheng Y., and Wang N., (2020). "Multilayer-structured fibrous membrane with directional moisture transportability and thermal radiation for high-performance air filtration," *e-Polymers*, vol. 20, no. 1, pp. 282-291.

Yin, L., Qu, G., Guo, P., Zhang, R., Sun, J. & Chen, D. (2019). Construction and enhanced low-temperature H_2S-sensing performance of novel hierarchical CuO@ WO_3 nanocomposites. *Journal of Alloys and Compounds*, 785, 367-373.